The Role of Deformation in the Low and Intermediate Temperature Oxidation of a Binary Nickel-Chromium Alloy

Aaron Cooke, Emmanuelle A. Marquis[1]

Department of Materials Science and Engineering, University of Michigan, Ann Arbor, MI

Corresponding Author: emarq@umich.edu

Abstract

Nickel-based alloys are well suited for high temperature applications due to their retention of mechanical performance at elevated temperatures; however, these high temperatures are also conducive to accelerated oxidation in these alloys. Oxidation of these alloys can be mitigated by the addition of chromium to the alloy composition and the use of deformation that provides short-circuit diffusion pathways to the surface allowing the rapid formation of protective oxide scales. The beneficial effects of deformation on oxide scale protection have been widely observed in nickel alloy systems, but the fundamental mechanisms on the microscale and nanoscale remain poorly understood. We characterized alloy and scale microstructures developing in model Ni alloys with varying levels of deformation during oxidation at intermediate and high temperatures to establish a mechanistic understanding and advance the current framework for oxidation resistant alloy design.

1. Introduction

Chromium containing nickel-based alloys are often used in high temperature, high load applications such as jet engine and power plant turbines, and high temperature automotive parts due to their oxidation resistance as chromia formers and their retention of mechanical properties at elevated temperatures. In the nickel-chromium system, the type of oxide scale formed depends on a variety of factors including the chromium content, the oxidation temperature, and the processing conditions and resulting microstructure. For $Ni_{70}Cr_{30}$ (the alloy studied in this paper), it has been shown that at 600ºC both NiO and Cr_2O_3 will be formed from an electropolished alloy [1]. It is well established in industry that deformation can be used to reduce the oxidation rate of nickel-based alloys, but the mechanism by which this happens and the effect of different types of deformation are not well understood at this time [2].

2. Methods

High purity starting materials were arc melted using an Edmund Bühler GmbH arc melter to produce 10 gram buttons of atomic composition $Ni_{70}Cr_{30}$. These buttons were remelted 5 times during the arc melting process and were heated to 1200°C for 24 hours in argon gas to produce a more homogeneous sample. Some samples underwent a fifty-percent thickness reduction by cold rolling to yield samples with bulk deformation. All of the samples were then cut using a low-speed diamond saw to produce testable specimens from the buttons. For the bulk deformed (BD) specimens, the slices were ground on all sides to 600 grit and ground to 1200 grit on the surface to be observed. As for the surface deformed (SD) samples, grinding was done to 240 grit. The deformation-free electropolished (EP) samples were ground to 1200 grit followed by 3 μm diamond suspension. These samples were then electropolished in an electrolyte of 10 vol% perchloric acid in methanol at 30 V and -30 °C for 15s. All specimens were then sonicated in acetone and methanol before oxidation. Oxidation occurred in either a tube furnace for 50 hours at 600°C or 10 minutes at 900°C for the bulk deformed and electropolished samples or was done as thermogravimetric analysis (TGA) in a Netzsch STA 443 Thermogravimetric Analyzer at 900°C for 100 hours for all three sample conditions. Samples for the TGA followed the same processing steps but were polished on all sides. One bulk deformed sample was also oxidized at 900ºC for 5 hours. These specimens were then characterized on the Nova 200 Nanolab SEM/FIB, Helios 650 Nanolab SEM/FIB, or Helios G4 PFIB UXe (all Thermo Fisher) using

focused ion beam (FIB) to create cross sections and scanning electron microscopy (SEM) to observe and image the oxide growth and microstructural evolution. Energy-dispersive X-ray spectroscopy was used to confirm the type of oxide formed and used in conjunction with TEM to identify and measure areas of subsurface chromium depletion as well as areas of depletion next to grain boundaries which is not currently discussed in this paper.

3. Results

The bulk deformed samples exhibited slower oxidation rates when compared to the electropolished condition across a range of temperatures, which matches with the anticipated results. After oxidation, the surface of the deformed samples have a single, coherent layer of protective Cr_2O_3 that is composed of small polyhedral nodules. In contrast, the electropolished samples can exhibit a duplex scale of NiO and Cr_2O_3 or a single scale of Cr_2O_3 showing grain orientation dependent oxidation. In addition to the effects of deformation condition on the oxidation of the alloy, the oxidation temperature played a significant role in the oxidation rate, significance of the grain orientation dependence, and subsurface pore formation of the alloy.

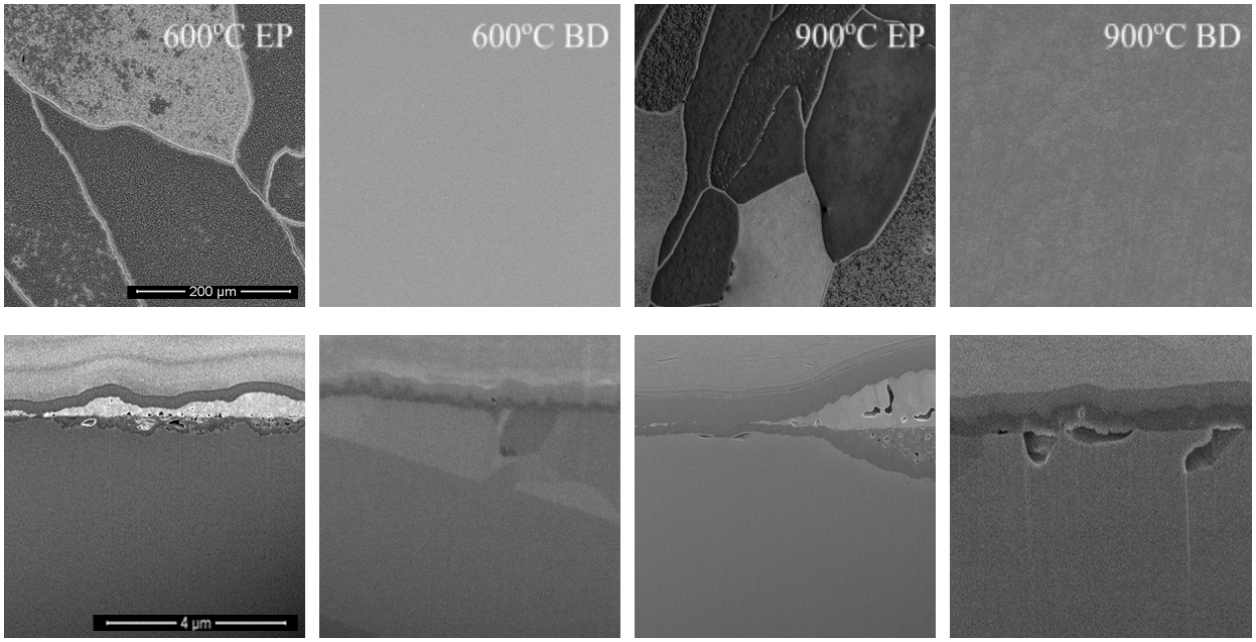

Figure 1. SEM micrographs showing the surface and cross section of the two deformation conditions (electropolished and bulk deformed) oxidized for 50 hours at 600°C or 10 minutes at 900°C in air. Images in the same row have the same magnification and use the same scale bar.

3.1 600°C Oxidation

After 50 hours at 600°C, the bulk deformed sample exhibited a single oxide scale of Cr_2O_3 with a thickness of 229 nm. In contrast, the electropolished scale forms a duplex scale with multiple oxides (NiO and Cr_2O_3) with varying thicknesses depending on location within the grain or along grain boundaries. The average thickness of the oxide was 585 nm where the oxide on the grain boundary was much thinner than on the bulk of the grain. In addition, there were bulbous nodules which increased the inherent variability of the oxide thickness. In addition to the differences in the oxide scale, there are differences under the scale. All samples undergo enough heating to recrystallize, so the bulk deformed sample's deep deformation exhibited a small-grained structure with a grain size of 2.9 microns after oxidation. In contrast, the electropolished sample had a mean grain size of 309.3 microns.

3.2 900°C Oxidation

The analysis of the 900°C oxidation for 10 minutes closely resembles that of the 600°C oxidation for 50 hours. The trends in oxide type and layering are the same as in the corresponding 600°C oxidation experiment, with a few points of differentiation. Even though the material was oxidized for only 10 minutes in comparison to the 50 hour oxidation, the oxides were thicker for both samples and the grains had grown to be larger for the deformed sample. The bulk deformed sample had an oxide thickness of 390 nm and a grain size of 4.3 microns while the electropolished sample had an average oxide thickness and grain size of 1736 nm and 254.2 microns respectively. The electropolished sample showed more evidence of grain orientation dependent oxidation and larger pore formation when compared to the 600°C oxidation.

3.3 Thermogravimetric Analysis

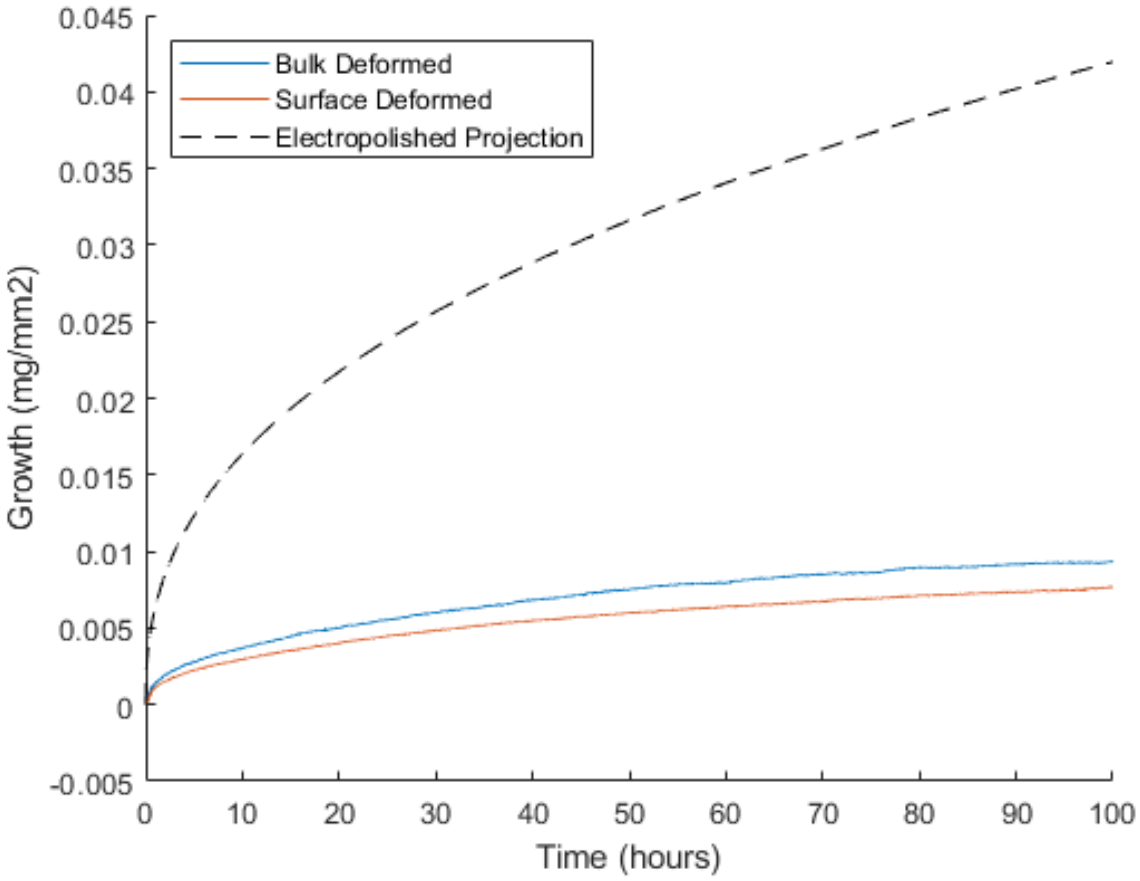

Figure 2. Mass gain plots of both bulk and surface deformed samples compared to a conservative model of the mass gain of a deformation free electropolished sample.

To confirm that the bulk deformed and surface deformed samples exhibit similar oxidation resistance, thermogravimetric analysis was performed. The oxidation behavior of this alloy (and many others) follows parabolic to near-parabolic behavior [3]. The data from the TGA has been fit to the equation $\Delta M = (C + K * t)^{1/m}$ where ΔM is the mass gain of the specimen normalized to its surface area, K is the rate constant, m is a fitting coefficient used to match the shape of the curve, and C is a constant. Note that when m equals 2, this equation becomes $\Delta M = (C + Kp * t)^{1/2}$ which is called the parabolic rate law [4]. In this case, K is replaced by Kp, the parabolic rate constant. The electropolished condition was projected using the mass gain calculated from the measured oxide thickness and the assumption that the oxide growth of the

samples of this condition is similar to the deformed samples and exhibits roughly parabolic behavior. This assumption is discussed further below.

4. Discussion

4.1 Grain Orientation Dependence

At both 600ºC and 900ºC, but more extensively at 900ºC, the alloy exhibits a dependence on the grain orientation during oxide growth. As seen in the cross section of the 900ºC EP panel of figure 1, the grains exhibit very different oxide morphologies with different thicknesses. In addition, a majority of the grains exhibit the duplex scale of NiO and Cr_2O_3 at 600ºC while the proportion of grains with each scale morphology is split more evenly at the higher temperature of oxidation. This indicates a stronger dependence on grain orientation during oxidation because differing grain structures are more likely to influence the oxide growth of the material. This type of anisotropy in diffusion and oxidation has been studied before in HCP alloys [5], but very little research has been done to show that anisotropy and grain orientation dependence is a major factor in FCC alloys like $Ni_{70}Cr_{30}$.

4.2 Pore Formation

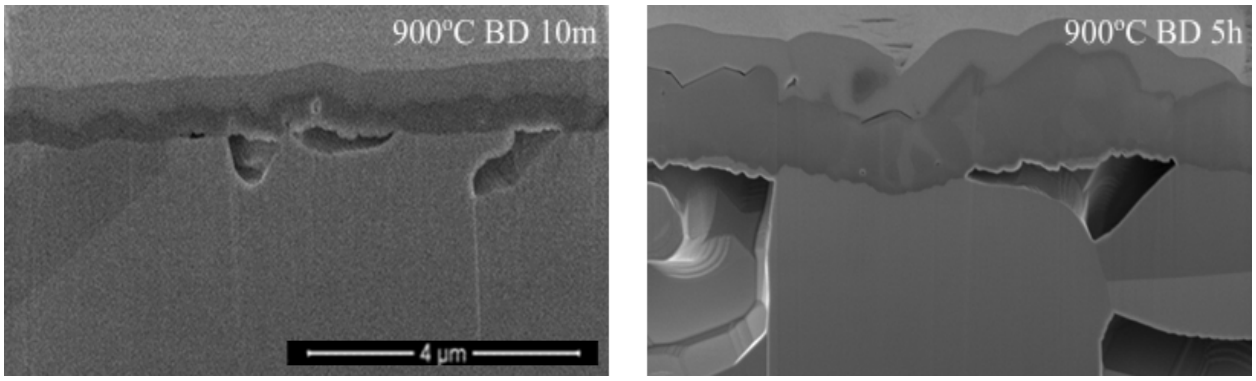

Figure 3. SEM micrographs of 900ºC samples at different oxidation times. Both images have the same magnification and use the same scale bar.

At 900ºC, the material exhibited subsurface pore deformation. The mechanism of high temperature pore formation has been investigated before [6]. The depth of the pore formation generally extends to the depth of subsurface chromium depletion in the sample. In addition, these pores tend to form at grain boundaries which is in agreement with the results of this study. It is a

plausible hypothesis to say that the pore depth and chromium depletion zone are related in these samples since the depletion in the sample is due to chromium diffusing to the surface to form the oxide scale and the diffusivity of chromium increases with increasing temperature. This also lends credence to grain boundaries serving as short circuit diffusion pathways [1]. As chromium is diffusing to the surface (at an elevated rate from grain boundaries), vacancies are left behind in the atomic sites these chromium atoms occupied. If these vacancies increase to the point of supersaturation, they can coalesce and form voids in regions of more depletion [6].

4.3 Thermogravimetric Analysis

When modeling the electropolished behavior of the electropolished condition, the choice was made to assume the growth behavior was parabolic. This most likely not the case due to the bulbous nature of the oxide scales and the differing oxidation morphologies at different points in the sample. However, this is the most conservative likely estimate of the oxide growth rate of the samples. Two other potential oxidation behaviors are linear and parabolic break away, both of which can apply if the oxide scale formed on the electropolished samples isn't protective, and these behaviors would have a much higher mass gain rate [7]. Even using the most conservative likely explanation, the deformed samples have an improvement on the oxidation resistance of this material of roughly one order of magnitude which is a critical improvement for many applications.

5. Conclusions

1. The $Ni_{70}Cr_{30}$ alloy exhibits heightened oxidation resistance from deformation when compared to undeformed samples.
2. This deformation effect is prevalent at both low (600^{o}C) and intermediate (900^{o}C) temperatures.
3. Intermediate temperatures result in much faster oxidation than low temperatures.
4. There is a higher grain orientation dependence of oxidation at intermediate temperatures than at low temperatures.
5. Pore growth is more prevalent and results in larger and deeper pores at intermediate temperatures when compared to low temperatures.

6. The deformed samples of both types show a near-parabolic behavior of oxide scale growth.

Acknowledgements

We would like to thank Thomas Valenza and Fei Xue along with the other members of the Marquis Lab for their constant support and acknowledge the University of Michigan College of Engineering for financial support and the Michigan Center for Materials Characterization for use of the instruments and staff assistance.

References

[1] F. Xue and E. A. Marquis, "Role of diffusion-induced grain boundary migration in the oxidation response of a ni-30 cr alloy," *Acta Materialia*, vol. 240, p. 118343, 2022.

[2] S. Leistikow, I. Wolf, and H. J. Grabke, "Effects of cold work on the oxidation behavior and carburization resistance of alloy 800," *Materials and Corrosion/Werkstoffe und Korrosion*, vol. 38, no. 10, pp. 556–562, 1987.

[3] M. Kemdehoundja, J. F. Dinhut, J. L. Grosseau-Poussard, and M. Jeannin, "High temperature oxidation of NI70CR30 alloy: Determination of oxidation kinetics and stress evolution in Chromia layers by Raman spectroscopy," *Materials Science and Engineering: A*, vol. 435-436, pp. 666–671, 2006.

[4] K. Chiang and T. Mintz, "Gravimetric techniques," *Techniques for Corrosion Monitoring*, pp. 239–254, 2021.

[5] X. Chen, L. Huang, Y. Jiao, S. Wang, Q. An, Y. Bao, and L. Geng, "Mechanisms of oxidation anisotropy between α-ti (0001) and $(01\bar{1}0)$ crystallographic planes in titanium matrix composites," *Materials Letters*, vol. 286, p. 129230, 2021.

[6] C. Desgranges, F. Lequien, E. Aublant, M. Nastar, and D. Monceau, "Depletion and voids formation in the substrate during high temperature oxidation of Ni–Cr alloys," *Oxidation of Metals*, vol. 79, no. 1-2, pp. 93–105, 2013.

[7] R. E. Smallman and A. H. W. Ngan, "Oxidation, corrosion and surface engineering," *Modern Physical Metallurgy*, pp. 617–657, 2014.